

# REPEATABILITY STUDY OF COMMERCIAL HARMONIC PHASE STANDARDS MEASURED BY A NONLINEAR VECTOR NETWORK ANALYZER\*

Jeffrey A. Jargon, Donald C. DeGroot, and Dominic F. Vecchia

National Institute of Standards and Technology  
325 Broadway, M/S 813.01  
Boulder, CO 80305, USA  
Tel: +1.303.497.3596 | Fax: +1.303.497.3970  
E-mail: jargon@boulder.nist.gov

## ABSTRACT

In this paper, we present the first published repeatability study of commercial harmonic phase standards (HPS) measured by a nonlinear vector network analyzer. Specifically, we measure two harmonic phase standards, one of which is specified to 20 GHz and the other to 50 GHz. By performing 5 calibrations and making 100 measurements from 600 MHz to 19.8 GHz at each calibration, we determine the repeatability bounds for the complex wave-variable vectors and associated phases and magnitudes of each harmonic component. We also compare the mean phase values to those supplied by the manufacturer. While we achieve standard uncertainties of no greater than  $0.73^\circ$ , we find significant variations in the mean values with changing HPS conditions and show evidence of a substantial thermal contribution.

## I. INTRODUCTION

A class of instruments known as nonlinear vector network analyzers (NVNA) are capable of characterizing nonlinear devices under realistic, large-signal operating conditions [1, 2]. To do this, complex traveling waves are measured at the ports of a device not only at the stimulus frequency (or frequencies), but also at other frequencies that are part of the large-signal response. Assuming the source signals are single-frequency time-harmonic waves and the device exhibits neither sub-harmonic nor chaotic behavior, the forward and reverse waves measured at the device boundaries will be combinations of the source signals, due to the nonlinearity of the device in conjunction with impedance mismatches between the system and the device. If a single excitation frequency is present, new frequency components may appear at all harmonics of the excitation frequency, and if multiple excitation frequencies are present, new frequency components may appear at the intermodulation products as well.

To capture this type of large-signal behavior, the calibration of a commercial NVNA consists of three steps: a relative calibration that is identical to that used in a linear vector network analyzer, an amplitude calibration that makes use of a power meter, and a phase distortion calibration that makes use of a harmonic phase standard. All are performed on a frequency grid related to the source tones and the anticipated nonlinear response of the device.

---

\* Work of an agency of the U.S. Government. Not subject to U.S. Copyright.

The commercial harmonic phase standard (HPS), the main components of which are a power amplifier and a step recovery diode, is driven at a fundamental frequency and produces a harmonic series output signal. The HPS, which is used as a transfer standard, is characterized by a sampling oscilloscope, which in turn is characterized by a nose-to-nose calibration [3]. In this way we transfer the phase-dispersion calibration of an oscilloscope to “knowing” the phase relationship of each harmonic of the phase standard output signal.

In this paper, we present the first published repeatability study of commercial harmonic phase standards measured by an NVNA. We measure two harmonic phase standards, one of which is specified to 20 GHz and the other to 50 GHz. By performing multiple measurements and utilizing the propagation-of-errors method, we determine the repeatability bounds for the complex wave-variable vectors and associated phases and magnitudes of each harmonic component. We compare our mean values to those supplied by the manufacturer. Upon finding significant time variations in our data, we also study the possibility of warm-up drift in the two devices.

## II. REPEATED CALIBRATIONS

Our repeatability study consisted of measuring two commercial harmonic phase standards (HPS), one of which is specified to 20 GHz and the other to 50 GHz. In our first set of experiments, we performed five back-to-back coaxial Open-Short-Load-Thru (OSLT) calibrations on the NVNA from 600 MHz to 19.8 GHz in steps of 600 MHz and used the 20 GHz harmonic phase standard for the phase dispersion calibration. We then made 100 repeated measurements of both harmonic phase standards at each calibration.

Figure 1 contains scatter plots of 100 measured values of  $b_1$  at 0.6, 6, 12, and 18 GHz for the 20 GHz HPS using the first calibration. At 600 MHz, all of the measurements lie along a diagonal line. The reason for this is that the commercial system software aligns the measured signals by adjusting the phase of the fundamental frequency waves so that the fundamental is always set to a prescribed value at a specified port. In this case, we chose  $151.88^\circ$  at port 1 since the manufacturer chose this phase reference for the values they provided. Doing so allows us to easily compare our measured values to theirs. Figure 2 contains scatter plots of 100 measured values at the same frequencies for the 50 GHz HPS using the first calibration. Figures 1 and 2 reveal that the 20 GHz HPS appears to be slightly less noisy than the 50 GHz device. Note that on Figure 1, the vertical and horizontal axes span 0.001 V, while on Figure 2, they span 0.002 V. Also note the apparent correlation between the real and imaginary components at some of the harmonics. (We will discuss this later.) The scatter for both devices appears to increase somewhat as a function of frequency, but not dramatically so. As the magnitudes decrease with frequency, we anticipate the variation in the phase to increase more as a result of decreasing signal-to-noise than as a result of increased scatter in the complex-wave variables. Note that in all figures and tables the measured quantities are reported as ‘ $b_1$ .’ This is because the harmonic phase standards are connected to port 1 and we are measuring the outgoing wave  $b$  in units of peak voltage divided by 2. Furthermore, the measured values of  $b_1$  are corrected to account for the reflection coefficients of the devices. These corrections, however, have a very small effect in our well-matched system.

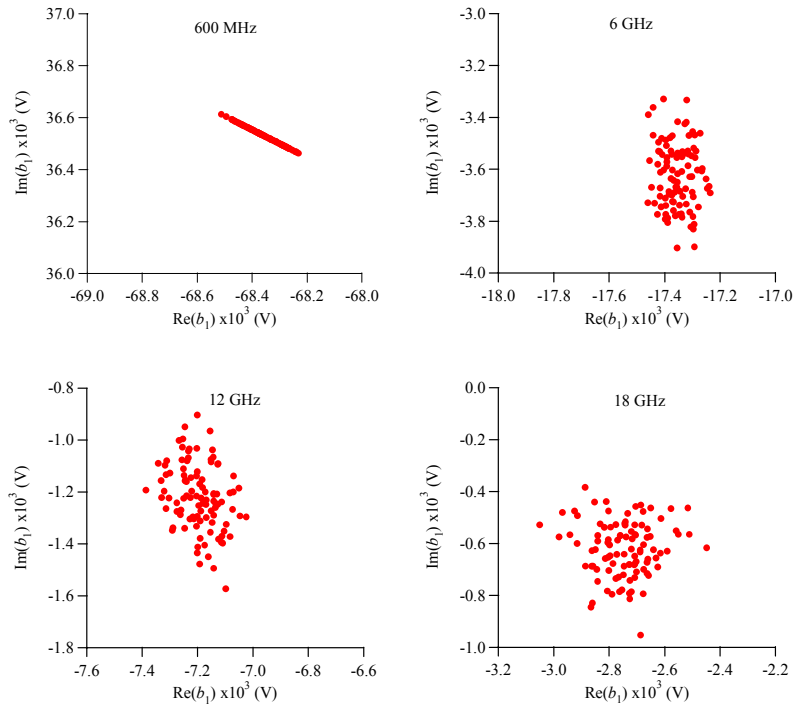


**Figure 1.** Scatter plots of 100 measured values of  $b_1$  at 0.6, 6, 12, and 18 GHz for one calibration made on the 20 GHz Harmonic Phase Standard.

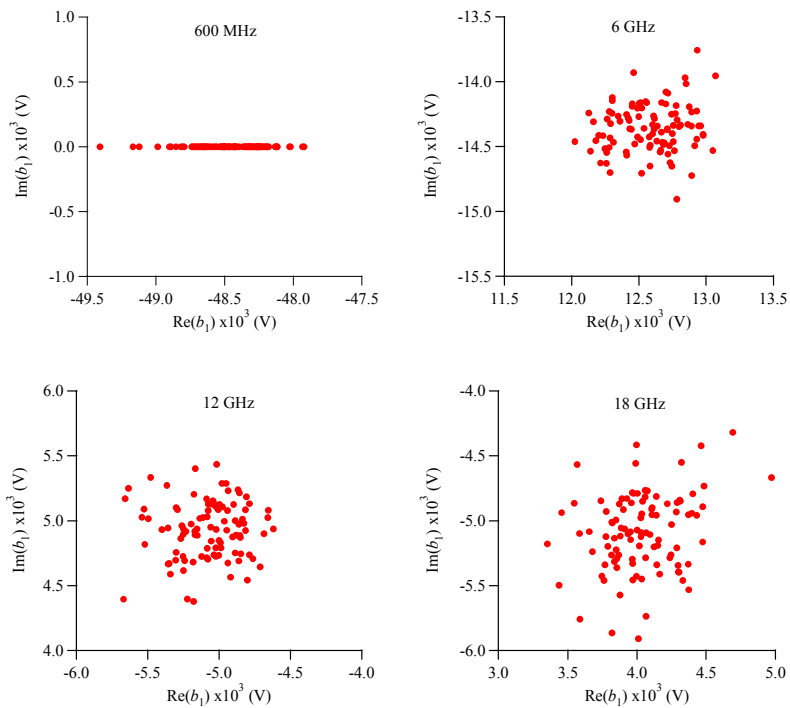


**Figure 2.** Scatter plots of 100 measured values of  $b_1$  at 0.6, 6, 12, and 18 GHz for one calibration made on the 50 GHz Harmonic Phase Standard.

Figures 3-6 show the magnitudes and phases of the 100 measured values for each of the five calibrations for the 20 GHz HPS, and Figures 7-8 show the magnitudes and phases of the 100 measured values at each of the five calibrations for the 50 GHz HPS. These figures illustrate how the devices vary with repeated measurements and calibrations. In general, the variations in the magnitudes and phases increase as the frequency increases for both devices, due to the respective decreasing signal-to-noise ratios.

Referring to Figure 5, we see that the measured phase angles for the 20 GHz HPS vary by up to  $15.32^\circ$  at 18 GHz for a single calibration. Here, we also see that the phase angles measured with the first calibration are markedly different from those measured in the subsequent calibrations. There is also significant drift from calibration to calibration. This is apparent in Figure 6, where we plot the phase angles of the 100 measured values consecutively at 18 GHz for each of the five calibrations. In this plot, we also see evidence of drift as a function of time within each calibration.

### III. STATISTICAL ANALYSIS

To get a more quantitative perspective, we conduct some basic statistical uncertainty analyses on our data. Since we are interested in the magnitudes and phase angles of the complex traveling wave variables, rather than the real and imaginary components, we utilize the propagation-of-errors (POE) method. Specifically, the formula

$$\sigma_z^2 = \left(\frac{\partial z}{\partial x}\right)^2 \sigma_x^2 + \left(\frac{\partial z}{\partial y}\right)^2 \sigma_y^2 + 2\frac{\partial z}{\partial x}\frac{\partial z}{\partial y}\sigma_{xy} \quad (1)$$

is used to calculate the approximate variance for a function  $z = g(x,y)$  of two measurement results  $x$  and  $y$  [4]. (In our case  $x$  and  $y$  correspond to the real and imaginary components of  $b_1$ ). The third term on the right side of the Equation (1) is necessary in situations where the  $x$  and  $y$  measurements may not be statistically independent. Since our commercial system software aligns the measured signals by adjusting the phase of the fundamental frequency waves so that the fundamental is always set to a prescribed value at a specified port, it is likely that the real and imaginary components of  $b_1$  are not completely independent after the phase alignment. We have, in fact, calculated correlation coefficients for our data and seen that they do contain low to moderate correlations. Furthermore, the phase alignment can affect the distributions of our measured data. So even if we begin with normally distributed data, it does not necessarily remain so after the phase alignment. Figure 9 shows a simple simulation we performed to illustrate this phenomenon using multiple measurements of signals at the fundamental frequency and the second harmonic. In Figure 9 (a), we simply rotate the phase of the fundamental signals by  $45^\circ$  and the second harmonic signals by a corresponding  $90^\circ$ , which preserves the distributions. In Figure 9 (b), however, we rotate the phase of the fundamental signals to align them each to  $0^\circ$ , like is done in our commercial system software, which causes the distribution of the second-harmonic signals to be skewed. We use equation (1) since it is useful even in the presence of the phase alignment that is performed on our measurements.

Particular formulas for calculating the POE standard deviations of our measured magnitudes and phase angles are presented below. If

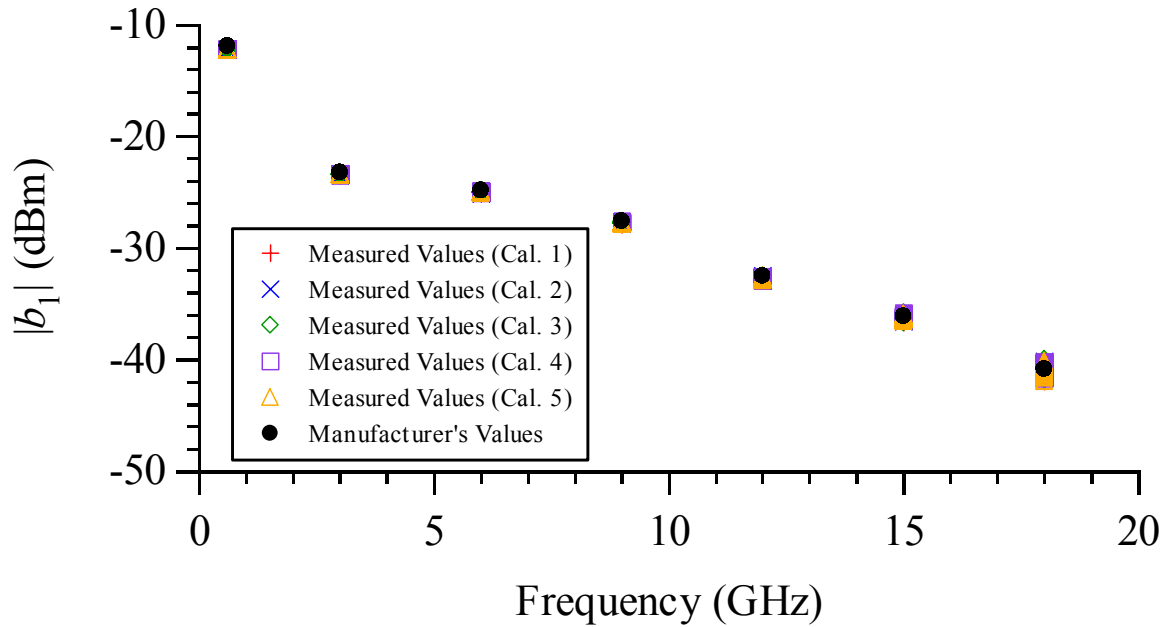


**Figure 3.** Magnitudes of the 100 measured values for each of the five calibrations along with the manufacturer's values for the 20 GHz Harmonic Phase Standard.

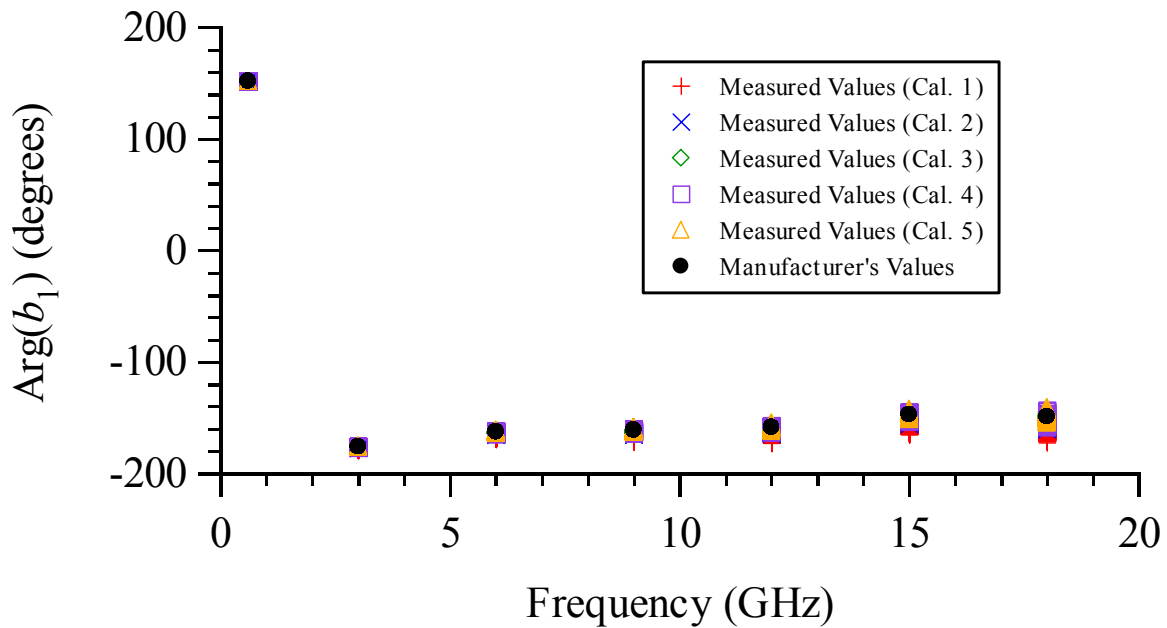


**Figure 4.** Phase angles of the 100 measured values for each of the five calibrations along with the manufacturer's values for the 20 GHz Harmonic Phase Standard.

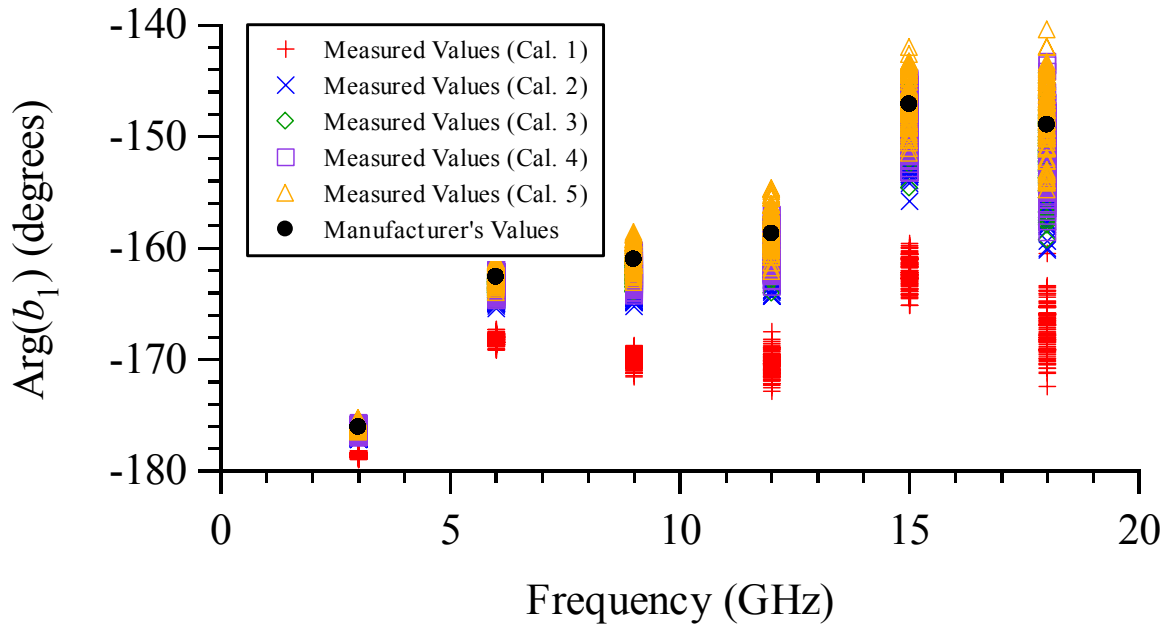


**Figure 5.** A closer view of the data presented in Figure 4. Phase angles of the 100 measured values for each of the five calibrations are shown along with the manufacturer's values for the 20 GHz Harmonic Phase Standard.

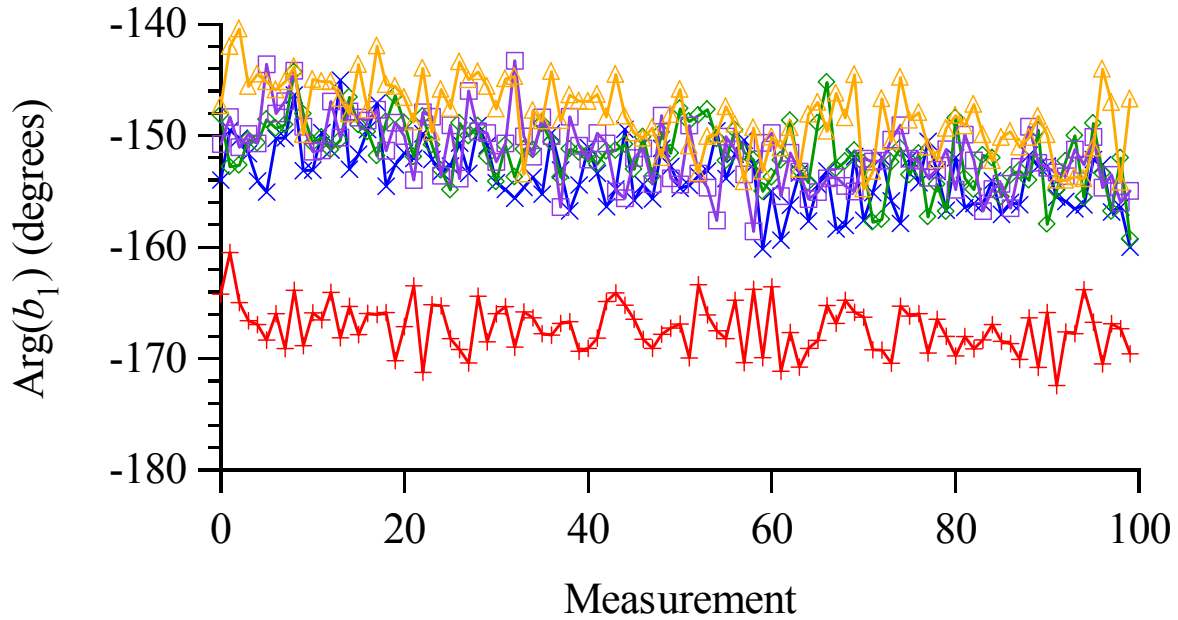


**Figure 6.** Phase angles of the 100 measured values at 18 GHz for each of the five calibrations made on the 20 GHz Harmonic Phase Standard.

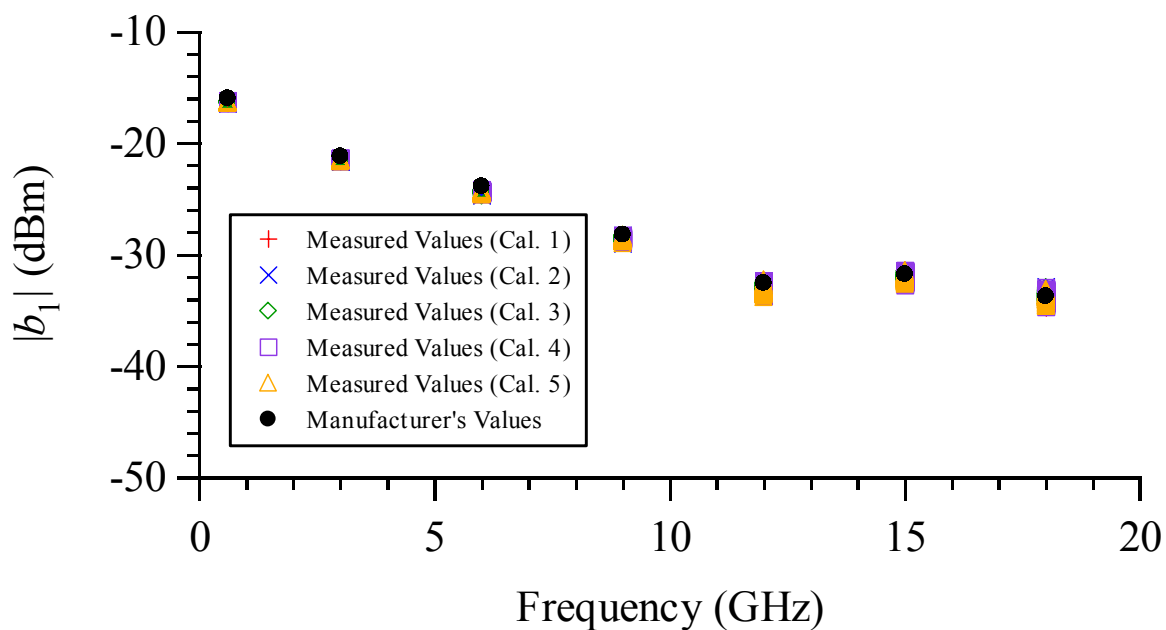


**Figure 7.** Magnitudes of the 100 measured values for each of the five calibrations along with the manufacturer's values for the 50 GHz Harmonic Phase Standard.

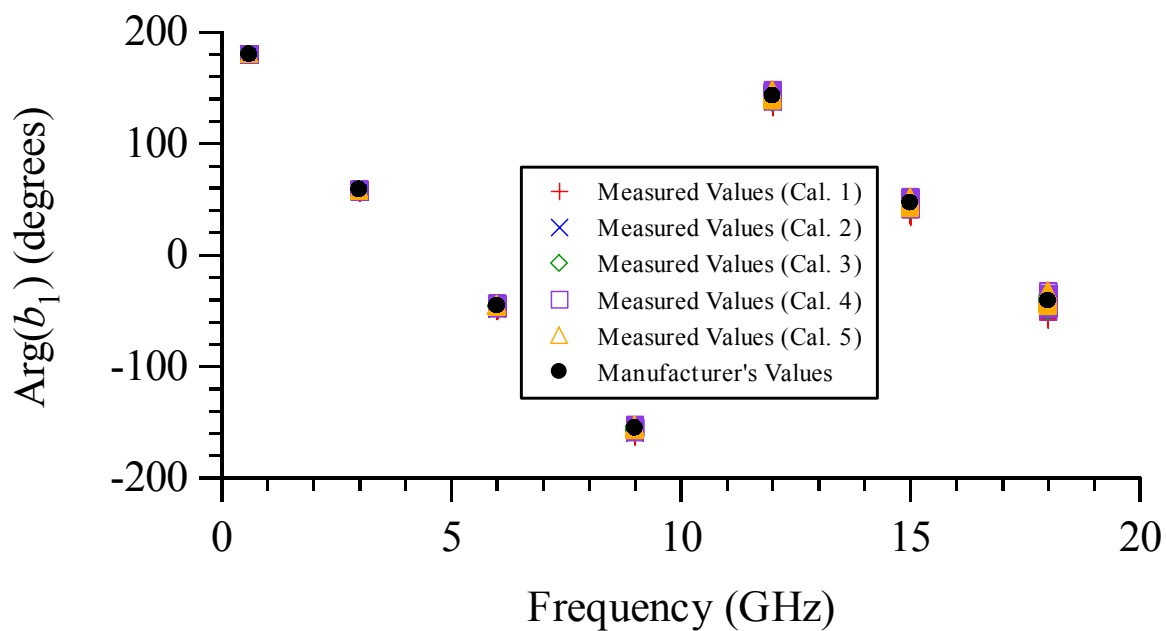


**Figure 8.** Phase angles of the 100 measured values for each of the five calibrations along with the manufacturer's values for the 50 GHz Harmonic Phase Standard.

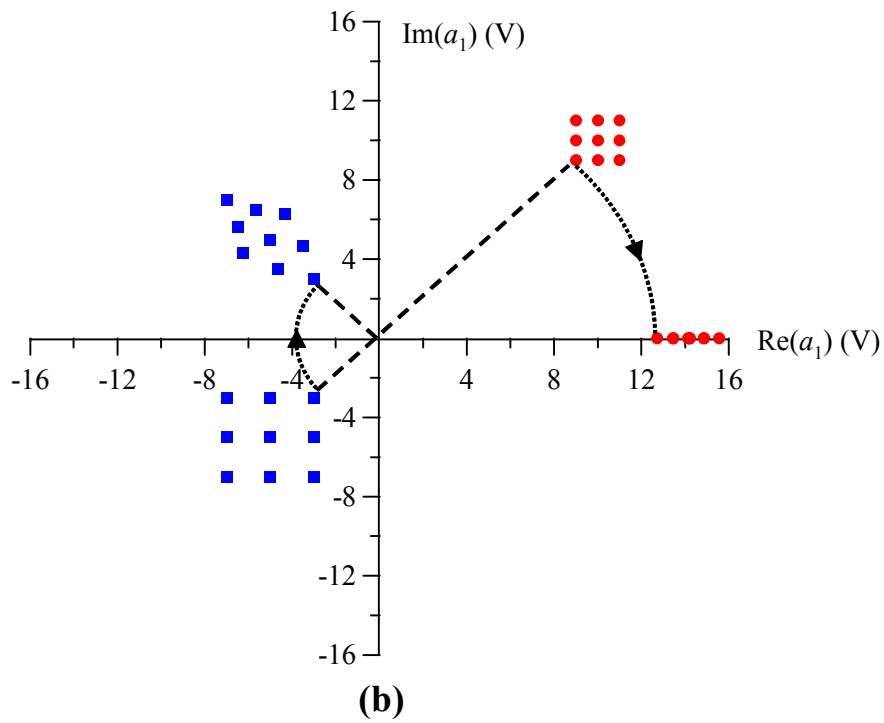
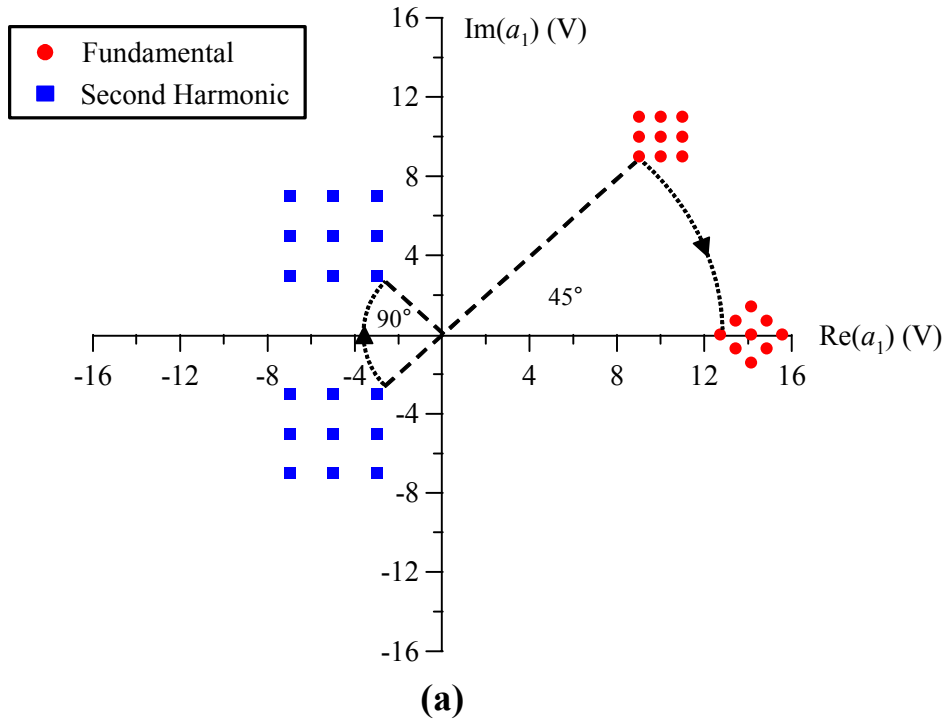


**Figure 9.** (a) Rotating the phase of the fundamental signals by  $45^\circ$  and the second harmonic signals by a corresponding  $90^\circ$  preserves the distributions. (b) Rotating the phase of the fundamental signals to align them each to  $0^\circ$  skews the distribution of the second-harmonic signals.

$$z_i = x_i + j y_i \quad (2)$$

denotes the  $i^{\text{th}}$  measurement of a complex-valued quantity, where  $i = 1, \dots, N$ , then we can define  $X$  as the mean of the  $x_i$ 's,  $Y$  as the mean of the  $y_i$ 's,  $S_x$  as the sample standard deviation of the  $x_i$ 's,  $S_y$  as the sample standard deviation of the  $y_i$ 's, and  $\rho$  as the sample correlation coefficient of the  $x_i$ 's to the  $y_i$ 's [4].

If we let

$$M = \sqrt{X^2 + Y^2} \quad (3)$$

be our estimate of the magnitude, then the sample standard deviation of the magnitude  $S_M$  can be calculated from the POE method, shown in equation (1), as

$$S_M = \frac{1}{\sqrt{N(X^2 + Y^2)}} \left[ X^2 S_x^2 + Y^2 S_y^2 + 2XY\rho S_x S_y \right]^{1/2}. \quad (4)$$

In addition, if we want the expanded uncertainty with 95% confidence, we can easily calculate it as

$$M \pm t_{N-1,0.975} S_M, \quad (5)$$

where  $t_{N-1,0.975}$  is the value of the Student's  $t$  distribution with  $N-1$  degrees of freedom and 95% confidence.

If we let

$$\phi = \tan^{-1}\left(\frac{Y}{X}\right) \quad (6)$$

be our estimate of the phase angle, we break up the problem into two steps. First, we take the ratio

$$R = \frac{Y}{X} \quad (7)$$

and determine the sample standard deviation of the ratio  $S_R$  from the propagation-of-errors method, shown in equation (1), as

$$S_R = \frac{Y}{\sqrt{NX}} \left[ \frac{S_y^2}{Y^2} + \frac{S_x^2}{X^2} - \frac{2\rho S_y S_x}{YX} \right]^{1/2}, \quad (8)$$

which is written in a form similar to that of reference [5]. In the next step, we take

$$\phi = \tan^{-1}(R) \quad (9)$$

and determine the sample standard deviation of the  $S_\phi$  from the POE method as

$$S_{\phi} = \left( \frac{1}{1 + R^2} \right) S_R . \quad (10)$$

In addition, if we want the expanded uncertainty with 95% confidence, we can easily calculate it as

$$\phi \pm t_{N-1, 0.975} S_{\phi} . \quad (11)$$

Tables 1 and 2 list the means and expanded uncertainties of the measured magnitudes and phase angles, as described in Equations (5) and (11), for the 20 GHz HPS. Tables 3 and 4 contain the corresponding computed values for the 50 GHz HPS.

For a single calibration, the expanded uncertainties in the magnitudes range from  $0.11 \times 10^{-4}$  V to  $0.23 \times 10^{-4}$  V for the 20 GHz device, and from  $0.31 \times 10^{-4}$  V to  $0.56 \times 10^{-4}$  for the 50 GHz device<sup>(1)</sup>. The expanded uncertainties in the phase angles range from  $1.75 \times 10^{-5}^\circ$  at 600 MHz to  $0.62^\circ$  at 18 GHz for the 20 GHz device, and range from  $0.52 \times 10^{-4}^\circ$  at 600 MHz to  $0.73^\circ$  at 18 GHz for the 50 GHz device. The reason that the standard deviations in the phase measurements are so small at 600 MHz is due to the phase alignment by the commercial system software. The calculated expanded uncertainties listed in the tables confirm that the 20 GHz HPS is slightly more repeatable in general up to 18 GHz than the 50 GHz device in both magnitude and phase. Also, the expanded uncertainties in the magnitudes and phases generally increase as the frequency increases for both devices due to the decreasing signal-to-noise ratios rather than increasing scattering in the complex plane.

We also compare our measured values to those supplied by the manufacturer of the harmonic phase standards. In Tables 5-8, we compute the differences between the means of our measured values at each calibration and the manufacturer's values for both harmonic phase standards. Here we see that the differences in phase for both devices are much larger in the first calibration, while the differences in magnitudes are relatively constant among all five calibrations. Figures 3-5 and 7-8 show the values supplied by the manufacturer along with the measured values. We see that our measurements tend to be consistently at the lower end of the manufacturer's values, oftentimes differing by more than one standard deviation from the composite mean. One possible reason for this is that the manufacturer's values for the 20 GHz harmonic phase reference, which we used in all five calibrations, were provided to us approximately three years ago, and the device's characteristics may have aged slightly in the meantime. Another possible reason may be due to the observed variability among calibrations.

We also carried out a second set of experiments where we performed another five back-to-back coaxial OSLT calibrations using the 50 GHz HPS this time rather than the 20 GHz HPS, and once again made 100 repeated measurements of both harmonic phase standards at each calibration. We do not have room to show those results in this paper, but they did repeat the behavior and trends of the first set of experiments.

---

<sup>(1)</sup> In our commercial NVNA, the software reports the  $a$  and  $b$  wave-variable vectors in units of peak-voltage divided by 2. This is due to the normalization which gives the wave-voltage equal to  $a+b$  and the wave-current equal to  $(a+b)/Z_{ref}$ .

**Table 1.** Means and expanded uncertainties of the measured magnitudes for the 20 GHz Harmonic Phase Standard.

Freq. (GHz)	$M \pm 1.982S_M$ $\times 10^4$ (V)				
	Cal. 1	Cal. 2	Cal. 3	Cal. 4	Cal. 5
0.6	$48.59 \pm 0.15$	$48.59 \pm 0.15$	$48.73 \pm 0.17$	$48.76 \pm 0.18$	$48.68 \pm 0.18$
3	$4.56 \pm 0.11$	$4.54 \pm 0.12$	$4.55 \pm 0.12$	$4.55 \pm 0.12$	$4.53 \pm 0.11$
6	$3.02 \pm 0.11$	$2.92 \pm 0.13$	$2.92 \pm 0.12$	$2.93 \pm 0.13$	$2.90 \pm 0.12$
9	$1.62 \pm 0.12$	$1.55 \pm 0.12$	$1.54 \pm 0.12$	$1.54 \pm 0.12$	$1.51 \pm 0.12$
12	$0.52 \pm 0.14$	$0.49 \pm 0.14$	$0.48 \pm 0.15$	$0.48 \pm 0.14$	$0.47 \pm 0.16$
15	$0.22 \pm 0.17$	$0.19 \pm 0.16$	$0.19 \pm 0.19$	$0.19 \pm 0.15$	$0.18 \pm 0.16$
18	$0.08 \pm 0.20$	$0.07 \pm 0.21$	$0.07 \pm 0.23$	$0.07 \pm 0.21$	$0.06 \pm 0.22$

**Table 2.** Means and expanded uncertainties of the measured phase angles for the 20 GHz Harmonic Phase Standard.

Freq. (GHz)	$\varphi \pm 1.982S_\varphi$ (deg.)				
	Cal. 1	Cal. 2	Cal. 3	Cal. 4	Cal. 5
0.6	$151.88 \pm 0.00$	$151.88 \pm 0.00$	$151.91 \pm 0.00$	$151.92 \pm 0.00$	$151.90 \pm 0.00$
3	$-178.59 \pm 0.04$	$-176.72 \pm 0.05$	$-176.46 \pm 0.05$	$-176.42 \pm 0.06$	$-175.94 \pm 0.06$
6	$-168.20 \pm 0.08$	$-164.06 \pm 0.11$	$-163.48 \pm 0.11$	$-163.45 \pm 0.13$	$-162.41 \pm 0.13$
9	$-169.95 \pm 0.13$	$-163.31 \pm 0.17$	$-162.36 \pm 0.17$	$-162.34 \pm 0.20$	$-160.72 \pm 0.20$
12	$-170.39 \pm 0.20$	$-161.79 \pm 0.26$	$-160.35 \pm 0.27$	$-160.41 \pm 0.29$	$-158.31 \pm 0.32$
15	$-162.17 \pm 0.25$	$-150.82 \pm 0.33$	$-149.35 \pm 0.30$	$-149.35 \pm 0.36$	$-146.54 \pm 0.40$
18	$-167.29 \pm 0.43$	$-153.59 \pm 0.56$	$-151.62 \pm 0.56$	$-151.64 \pm 0.59$	$-148.18 \pm 0.62$

**Table 3.** Means and expanded uncertainties of the measured magnitudes for the 50 GHz Harmonic Phase Standard.

Freq. (GHz)	$M \pm 1.982S_M$ $\times 10^4$ (V)				
	Cal. 1	Cal. 2	Cal. 3	Cal. 4	Cal. 5
0.6	$23.48 \pm 0.52$	$23.48 \pm 0.51$	$23.40 \pm 0.51$	$23.46 \pm 0.48$	$23.43 \pm 0.51$
3	$5.41 \pm 0.38$	$5.47 \pm 0.37$	$5.47 \pm 0.35$	$5.50 \pm 0.34$	$5.48 \pm 0.35$
6	$2.60 \pm 0.39$	$2.57 \pm 0.42$	$2.56 \pm 0.38$	$2.59 \pm 0.36$	$2.58 \pm 0.40$
9	$1.23 \pm 0.31$	$1.17 \pm 0.36$	$1.16 \pm 0.38$	$1.16 \pm 0.33$	$1.15 \pm 0.37$
12	$0.36 \pm 0.44$	$0.37 \pm 0.45$	$0.36 \pm 0.44$	$0.37 \pm 0.53$	$0.37 \pm 0.50$
15	$0.46 \pm 0.41$	$0.45 \pm 0.41$	$0.44 \pm 0.44$	$0.45 \pm 0.53$	$0.45 \pm 0.43$
18	$0.30 \pm 0.50$	$0.30 \pm 0.48$	$0.30 \pm 0.51$	$0.30 \pm 0.56$	$0.30 \pm 0.50$

**Table 4.** Means and expanded uncertainties of the measured phase angles for the 50 GHz Harmonic Phase Standard.

Freq. (GHz)	$\varphi \pm 1.982S_\varphi$ (deg.)				
	Cal. 1	Cal. 2	Cal. 3	Cal. 4	Cal. 5
0.6	180.01 ± 0.00	180.01 ± 0.00	180.01 ± 0.00	180.01 ± 0.00	180.01 ± 0.00
3	56.59 ± 0.07	57.89 ± 0.07	57.93 ± 0.07	58.22 ± 0.08	58.10 ± 0.06
6	-48.80 ± 0.14	-45.96 ± 0.17	-45.90 ± 0.15	-45.29 ± 0.16	-45.53 ± 0.13
9	-160.38 ± 0.23	-155.85 ± 0.26	-155.72 ± 0.25	-154.96 ± 0.27	-155.04 ± 0.23
12	135.80 ± 0.37	141.68 ± 0.39	141.97 ± 0.46	142.85 ± 0.43	142.54 ± 0.40
15	38.11 ± 0.37	45.83 ± 0.40	46.18 ± 0.50	47.36 ± 0.45	47.30 ± 0.43
18	-51.22 ± 0.55	-41.78 ± 0.57	-41.62 ± 0.73	-40.04 ± 0.66	-39.80 ± 0.61

**Table 5.** Differences between the means of the measured magnitudes and the manufacturer's values for the 20 GHz Harmonic Phase Standard.

Freq. (GHz)	$\Delta_M$ (V)				
	Cal. 1	Cal. 2	Cal. 3	Cal. 4	Cal. 5
0.6	$-3.61 \times 10^{-4}$	$-3.61 \times 10^{-4}$	$-3.47 \times 10^{-4}$	$-3.44 \times 10^{-4}$	$-3.52 \times 10^{-4}$
3	$-1.70 \times 10^{-5}$	$-1.81 \times 10^{-5}$	$-1.80 \times 10^{-5}$	$-1.79 \times 10^{-5}$	$-1.93 \times 10^{-5}$
6	$2.15 \times 10^{-7}$	$-8.42 \times 10^{-6}$	$-9.68 \times 10^{-6}$	$-8.16 \times 10^{-6}$	$-1.15 \times 10^{-5}$
9	$5.39 \times 10^{-6}$	$-1.35 \times 10^{-6}$	$-2.39 \times 10^{-6}$	$-2.15 \times 10^{-6}$	$-5.24 \times 10^{-6}$
12	$2.31 \times 10^{-6}$	$-9.42 \times 10^{-7}$	$-1.66 \times 10^{-6}$	$-1.68 \times 10^{-6}$	$-2.85 \times 10^{-6}$
15	$2.87 \times 10^{-6}$	$3.18 \times 10^{-7}$	$-1.01 \times 10^{-7}$	$7.91 \times 10^{-8}$	$-5.86 \times 10^{-7}$
18	$1.09 \times 10^{-6}$	$2.41 \times 10^{-7}$	$9.66 \times 10^{-8}$	$1.25 \times 10^{-7}$	$-2.08 \times 10^{-7}$

**Table 6.** Differences between the means of the measured phase angles and the manufacturer's values for the 20 GHz Harmonic Phase Standard.

Freq. (GHz)	$\Delta_\varphi$ (deg.)				
	Cal. 1	Cal. 2	Cal. 3	Cal. 4	Cal. 5
0.6	0.00	0.00	0.03	0.04	0.02
3	-2.52	-0.64	-0.39	-0.34	0.13
6	-5.58	-1.44	-0.86	-0.82	0.21
9	-8.91	-2.27	-1.32	-1.30	0.31
12	-11.65	-3.05	-1.61	-1.67	0.42
15	-15.05	-3.70	-1.98	-2.24	0.57
18	-18.31	-4.61	-2.64	-2.66	0.79

**Table 7.** Differences between the means of the measured magnitudes and the manufacturer’s values for the 50 GHz Harmonic Phase Standard.

Freq. (GHz)	$\Delta_M$ (V)				
	Cal. 1	Cal. 2	Cal. 3	Cal. 4	Cal. 5
0.6	$-1.84 \times 10^{-4}$	$-1.84 \times 10^{-4}$	$-1.92 \times 10^{-4}$	$-1.86 \times 10^{-4}$	$-1.89 \times 10^{-4}$
3	$-5.37 \times 10^{-5}$	$-4.69 \times 10^{-5}$	$-4.78 \times 10^{-5}$	$-4.39 \times 10^{-5}$	$-4.61 \times 10^{-5}$
6	$-3.08 \times 10^{-5}$	$-3.35 \times 10^{-5}$	$-3.43 \times 10^{-5}$	$-3.17 \times 10^{-5}$	$-3.25 \times 10^{-5}$
9	$-4.03 \times 10^{-6}$	$-1.04 \times 10^{-5}$	$-1.11 \times 10^{-5}$	$-1.15 \times 10^{-5}$	$-1.19 \times 10^{-5}$
12	$-5.04 \times 10^{-6}$	$-4.17 \times 10^{-6}$	$-4.41 \times 10^{-6}$	$-4.04 \times 10^{-6}$	$-4.30 \times 10^{-6}$
15	$-1.15 \times 10^{-6}$	$-2.36 \times 10^{-6}$	$-2.58 \times 10^{-6}$	$-2.32 \times 10^{-6}$	$-2.55 \times 10^{-6}$
18	$6.54 \times 10^{-8}$	$-1.80 \times 10^{-7}$	$-5.49 \times 10^{-7}$	$-1.26 \times 10^{-7}$	$-4.70 \times 10^{-7}$

**Table 8.** Differences between the means of the measured phase angles and the manufacturer’s values for the 50 GHz Harmonic Phase Standard.

Freq. (GHz)	$\Delta_\phi$ (deg.)				
	Cal. 1	Cal. 2	Cal. 3	Cal. 4	Cal. 5
0.6	0.01	0.01	0.01	0.01	0.01
3	-2.29	-1.00	-0.95	-0.67	-0.78
6	-3.38	-0.53	-0.48	0.14	-0.10
9	-5.42	-0.89	-0.76	0.00	-0.09
12	-7.14	-1.25	-0.96	-0.07	-0.39
15	-8.77	-1.05	-0.70	0.49	0.42
18	-10.45	-1.01	-0.85	0.73	0.97

#### IV. WARM-UP DRIFT

As mentioned earlier, we found some evidence of a long time-constant drift within individual calibrations, as shown in Figure 6. So, our next experiment was to look more closely at this possibility. After one calibration, we made 1000 repeated measurements of the 20 GHz HPS with a five-second pause between each measurement. Before starting, however, we set the source on to -80 dBm for approximately thirty minutes in an attempt to separate out any possible warm-up of the source from that of the HPS. Figure 10 shows the measured phase angles for the 1000 consecutive measurements. It is obvious that there is considerable drift, with up to a 49.22° span for the measurements at 18 GHz. By performing calculations on the various curves, we find a  $1/e$  time-constant of approximately 500 seconds, which is much longer than the warm-up time of 120 seconds set by the manufacturer’s control software and much shorter than the time required to reach stability.

We repeated this experiment with the 50 GHz HPS. Figure 11 shows the phase angles for the 1000 consecutive measurements. Here, the phase angles at each frequency were shifted so

they could all be viewed on the same graph. Once again, we see considerable drift, although not quite as pronounced as with the 20 GHz HPS. There is a span, however, of up to  $34.41^\circ$  for the measurements at 18 GHz. And once again, we find a  $1/e$  time-constant of approximately 500 seconds.

We measured the time-evolution of the port impedance during these experiments and did not observe a significant drift. Further, we have not observed a drift of this magnitude in other long-term repeatability studies conducting on our system with other types of devices. We submit these data as evidence for a long-term time-constant thermal effect in our HPS's.

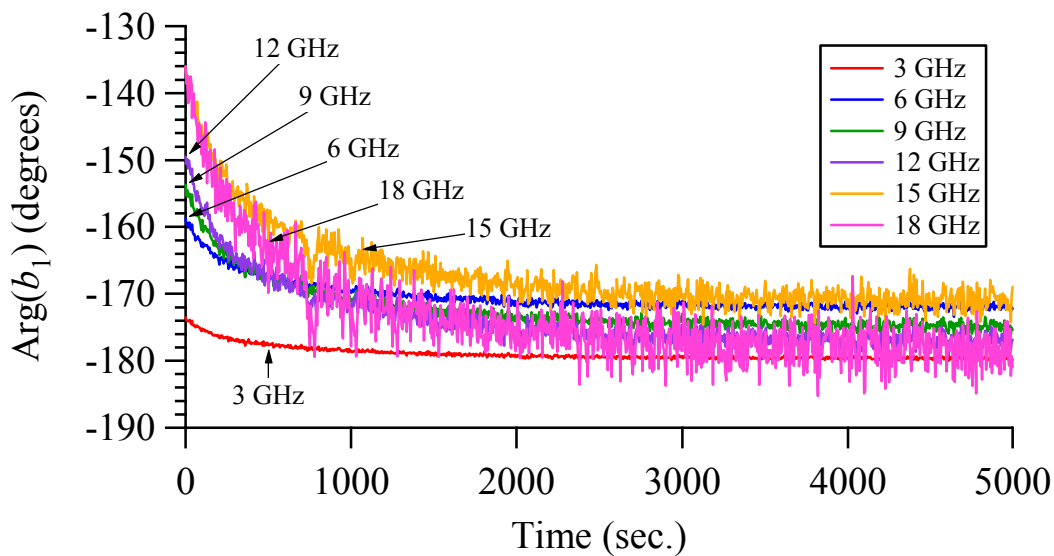


**Figure 10.** Phase angles of one-thousand consecutive measurements made every 5 seconds on the 20 GHz Harmonic Phase Standard.

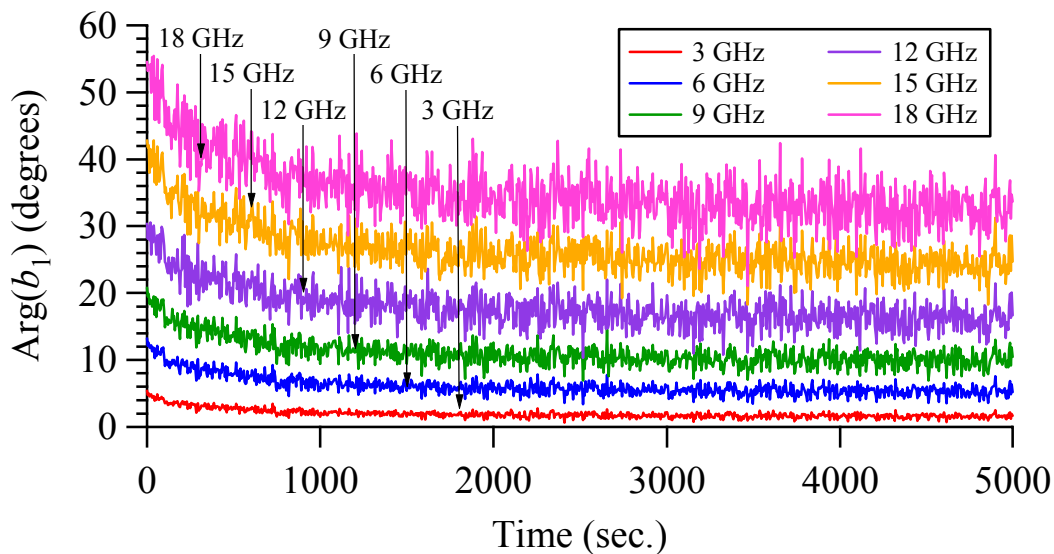


**Figure 11.** Shifted phase angles of one-thousand consecutive measurements made every 5 seconds on the 50 GHz Harmonic Phase Standard.

## V. CONCLUDING REMARKS

In this paper, we presented a repeatability study of commercial harmonic phase standards measured by an NVNA. We measured two harmonic phase standards, one of which is specified to 20 GHz and the other to 50 GHz. By performing five calibrations and making 100 measurements at each calibration, we determined the repeatability bounds for the complex wave-variable vectors and associated phases and magnitudes of each harmonic component by utilizing the propagation-of-errors method to compute expanded uncertainties. We found that the expanded uncertainties of the magnitudes and phases generally increase as the frequency increases for both devices due to the decreasing signal-to-noise ratios. We discovered that the 20 GHz HPS is slightly more repeatable in general up to 18 GHz than the 50 GHz device. The expanded uncertainties of the measured phase angles for a single calibration were no greater than  $0.62^\circ$  for the 20 GHz HPS and no greater than  $0.73^\circ$  for the 50 GHz HPS.

We compared our mean values to those supplied by the manufacturer and found our measurements to be consistently lower than the manufacturer's values at the higher frequencies, oftentimes differing by more than one standard deviation from the composite mean. Once again, a possible reason for this is that the manufacturer's values for the 20 GHz harmonic phase reference, which we used in all five calibrations, were provided to us approximately three years ago, and the device's characteristics may have aged slightly in the meantime. Another possible reason may be a long thermal time-constant effect in our harmonic phase standards.

Finally, we studied the possibility of warm-up drift in the two devices. We noticed considerable drift as a function of time, with an estimated  $1/e$  time-constant of around 500 seconds, which is much longer than the warm-up time of 120 seconds set by the manufacturer's control software.

We should reiterate that in this study we used the commercial system software to align the measured signals by adjusting the phase of the fundamental frequency waves so that the fundamental was always set to a prescribed value at a specified port. Other, more sophisticated, alignment methods may result in different distributions of the measured complex wave-variable vectors, which could in turn influence the uncertainties to some degree. On the other hand, these different alignment techniques could mask some of the thermal drift we observed. Future work will include studying the extent of these effects.

We should also mention that this study complements a previous report by Remley [6], where she performed a sensitivity study of the effect of the variation of sampling-circuit parameters on the phase error in the nose-to-nose calibration using a SPICE model of the sampling circuit. Interestingly enough, contributions from both uncertainties are of roughly the same order. With uncertainty values for the nose-to-nose calibration and the repeatability bounds, we are closer to estimating an overall phase uncertainty in NVNA measurements, linked to the nose-to-nose method.

## ACKNOWLEDGMENT

The authors thank Frans Verbeyst for reviewing our manuscript and providing many helpful comments.

## REFERENCES

- [1] J. Verspecht, P. Debie, A. Barel, and L. Martens, "Accurate on wafer measurement of phase and amplitude of the spectral components of incident and scattered voltage waves at the signal ports of a nonlinear microwave device," *1995 IEEE MTT-S Int. Microwave Symp. Dig.*, vol. 3, pp. 1029-1032, May 1995.
- [2] J. Verspecht, "Calibration of a measurement system for high-frequency nonlinear devices," Doctoral Dissertation, Vrije Universiteit Brussel, Brussels, Belgium, 1995.
- [3] J. Verspecht and K. Rush, "Individual characterization of broadband sampling oscilloscopes with a nose-to-nose calibration procedure," *IEEE Transactions on Instrumentation and Measurement*, vol. 43, no. 2, pp. 347-354, April 1994.
- [4] H. H. Ku, "Notes on the use of propagation of error formulas," *Journal of Research of the National Bureau of Standards – C. Engineering and Instrumentation*, vol. 70C, no. 4, Oct. – Dec. 1966.
- [5] J. Hannig, C. M. Wang, and H. K. Iyer, "Uncertainty calculation for the ratio of dependent measurements," *Metrologia*, vol. 40, pp. 177-183, June 2003.
- [6] K. A. Remley, "Nose-to nose oscilloscope calibration phase error inherent in the sampling circuitry," *60<sup>th</sup> ARFTG Conference Digest*, pp. 85-97, December 2002.